Bioconjugate Chemistry

Article

pubs.acs.org/bc

IF7-Conjugated Nanoparticles Target Annexin 1 of Tumor Vasculature against P-gp Mediated Multidrug Resistance

De-Hong Yu,[†,‡,#] Ya-Rong Liu,[‡,#] Xin Luan,[‡] Hai-Jun Liu,[‡] Yun-Ge Gao,[‡] Hao Wu,[†] Chao Fang,*[,‡] and Hong-Zhuan Chen*[,‡]

[†]Department of Otolaryngology-Head and Neck Surgery, Xinhua Hospital, Ear Institute, Shanghai Jiao Tong University School of Medicine, Shanghai Key Laboratory of Translational Medicine on Ear and Nose diseases, 1665 Kong Jiang Road, Shanghai 200092, China

[‡]Hongqiao International Institute of Medicine, Shanghai Tongren Hospital and Department of Pharmacology, Institute of Medical Sciences, Shanghai Jiao Tong University School of Medicine, 280 South Chongqing Road, Shanghai 200025, China

ABSTRACT: Multidrug resistance is the main cause of clinical chemotherapeutic failure. Antiangiogenic cancer therapy with nanomedicine that allows the targeted delivery of antiangiogenic agents to tumor endothelial cells may contribute to innovative strategies for treating multidrug-resistant cancers. In this study, we developed a new nanodrug delivery system (nano-DDS), with improved antiangiogenic efficacy against multidrug resistant human breast cancer MCF-7/ADR cells. Here, the IF7 ligand was a peptide designed to bind the annexin 1 (Anxa 1), a highly specific marker of the tumor vasculature surface, with high affinity and specificity. IF7-conjugated Anxa 1-targeting nanoparticles containing paclitaxel (IF7-PTX-NP) allowed controlled drug release and displayed favorable prolonged circulation in vivo. IF7-PTX-NP was significantly internalized by human umbilical vein endothelial cells (HUVEC) through the IF7-Anxa 1 interaction, and this facilitated uptake enhanced the expected antiangiogenic activity of inhibiting HUVEC proliferation, migration, and tube formation in a Matrigel plug relative to those of Taxol and PTX-NP. As IF7-PTX-NP targeted the tumor vessels, more nanoparticles accumulated in MCF-7/ADR tumors, and more importantly, induced significant apoptosis of the tumor vascular endothelial cells and necrosis of the tumor tissues. Low dose paclitaxel (1 mg/kg) formulated in IF7-PTX-NP showed significant anticancer efficacy, delaying the growth of MCF-7/ADR tumors. The same efficacy was only obtained with an 8-fold dose of paclitaxel (8 mg/kg) as Taxol plus XR9576, a potent P-gp inhibitor. The anticancer efficacy of IF7-PTX-NP was strongly associated with the improved antiangiogenic effect, evident as a dramatic reduction in the tumor microvessel density and pronounced increase in apoptotic tumor cells, with no obvious toxicity to the mice. This nano-DDS, which targets the tumor neovasculature, offers a promising strategy for the treatment of multidrug-resistant cancer.

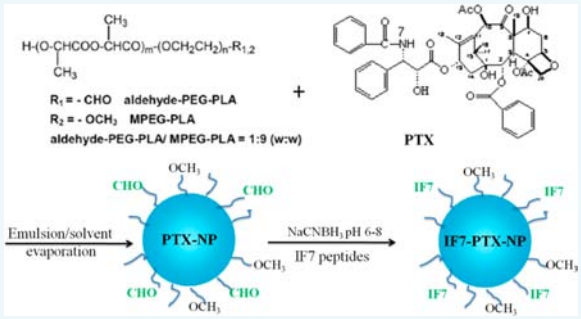

INTRODUCTION

Multidrug resistance (MDR) is one of the major obstacles to the successful clinical treatment of various types of cancer. The mechanisms depend on various factors, including enzyme inactivation, ATP-binding cassette (ABC) transporters responsible for drug efflux pumps (i.e., P-glycoprotein [P-gp], multidrug resistance proteins, and breast cancer resistant protein), or the dysregulation of DNA repair. As angiogenesis is one of the distinct hallmarks of cancer, antiangiogenic cancer therapy is emerging as a promising strategy to combat drug resistance.[1−3] Several antiangiogenic drugs have been approved by the U.S. Food and Drug Administration and successfully translated into the clinical context for various cancers.[4−6] There are several advantages of targeting endothelial cells (ECs) to inhibit tumor angiogenesis compared with conventional chemotherapy, which directly targets cancer cells to inhibit their proliferation or induce their death.[7] First, a significant "bystander effect" can be expected because each vessel capillary supports the survival and growth of hundreds of tumor cells. Second, tumor vascular ECs are directly exposed to the blood circulation, and are more easily reached than tumor cells, especially those in the deeper tumor parenchyma. Third, drug resistance resulting from genetic and epigenetic mechanisms often reduces the effectiveness of available drugs. Antiangiogenic therapy targets the genetically stable ECs of the tumor vasculature, and therefore potentially reduces the incidence of drug resistance.[7]

The specific delivery of chemotherapeutic agents to tumor vessels using nanoparticulate drug delivery systems (nano-DDS) that actively targets tumor vascular ECs offers the significant advantages of reducing off-target adverse effects, reducing the cumulative dose, and enhancing the efficacy of tumor vessel targeting without compromising antitumor efficacy.[8−10] Nano-DDS allow the site-specific delivery of

Received: May 19, 2015
Revised: June 13, 2015
Published: June 15, 2015

DOI: 10.1021/acs.bioconjchem.5b00283
Bioconjugate Chem. 2015, 26, 1702−1712

traditional chemotherapeutic agents to predetermined positions. At present, nanoparticle-mediated active targeting of the tumor vasculature with antiangiogenic agents has been achieved by targeting the vascular endothelial growth factor (VEGF) receptors (VEGFRs), $\alpha_v\beta_3$ integrins, and aminopeptidase N (CD13) .[11−13] For instance, a metronomic chemotherapy with SP5.2-DTX-NP targets Flt-1 has displayed superior antitumor efficacy, with significantly prolonged survival and minimal toxicity.[14]

Recently, annexin 1 (Anxa 1) was identified with a rigorous subtractive proteomic analysis as a novel specific biomarker expressed on the surfaces of tumor vasculature ECs.[15] In *Anxa1*-null mice, tumor growth was significantly suppressed by the lack of angiogenesis, suggesting that Anxa 1 is essential for tumor angiogenesis.[16] The expression of Anxa1 in the tumor vasculature is apparently universal to all tumor types in mice and humans,[16] strongly implicating it as a therapeutic biomarker for tumor vasculature-targeting vehicles. A peptide designated IF7 (IFLLWQR), isolated from a phage display peptide library, was found to bind Anxa 1 with high affinity and specificity. Moreover, the IF7 peptide conjugated to the potent anticancer drug SN-38 and injected intravenously into nude mice carrying human colon HCT116 tumors efficiently suppressed tumor growth.[15,17] We speculated that this peptide could be used as an effective ligand for nano-DDS that actively target the tumor vasculature.

In this study, we developed a novel nano-DDS of IF7-peptide-conjugated NP loading paclitaxel (PTX, a potent antiangiogenic model drug)[18,19] designated IF7-PTX-NP, to improve the drug's antiangiogenic efficacy, reduce the dose-associated adverse effects, and promote its antitumor efficacy. We investigated the ECs uptake and antiangiogenic activity of the nano-DDS in vitro, in vivo pharmacokinetics, targeting of the tumor vasculature in vivo, the paclitaxel-induced apoptosis of tumor ECs, and the necrosis of tumor tissues treated with IF7-PTX-NP. We also hypothesized that this tumor-vessel-targeting nano-DDS could potentially treat resistant cancers by targeting tumor ECs rather than the resistant tumor cells. The human breast cancer MCF-7/ADR cells, which display the drug-induced expression of P-gp on the cell surface,[20] were chosen to establish a multidrug-resistant cancer model. The capacity of IF7-PTX-NP to target tumor ECs and treat resistant MCF-7/ADR tumor xenografts in mice was investigated.

RESULTS

Characteristics of IF7-PTX-NP. IF7-PTX-NP was fabricated with the emulsion and solvent evaporation method, with subsequent surface functionalization, as described in the Experimental Procedures (Figure 1A). No marked differences were observed in the morphologies and particle size of IF7-PTX-NP and PTX-NP (Figure 1B−E). A representative transmission electron microscopy (TEM) micrograph showed that IF7-PTX-NP were spherical in shape with a smooth surface, with no aggregation or adhesion (Figure 1B). The physicochemical characteristics of the nanoparticles are summarized in Table 1. The size of IF7-PTX-NP was uniformly 92.68 ± 8.68 nm in the TEM images. In the dynamic light scattering (DLS) assay, the size of IF7-PTX-NP fitted a Gaussian distribution well (i.e., normal distribution) and the number-based particle size was 156.43 ± 25.41 nm, much higher than that observed with TEM (Figure 1B and D).

As shown in Table 1, the zeta potential of IF7-PTX-NP was −15.67 ± 1.53 mV, which is significantly higher than that of

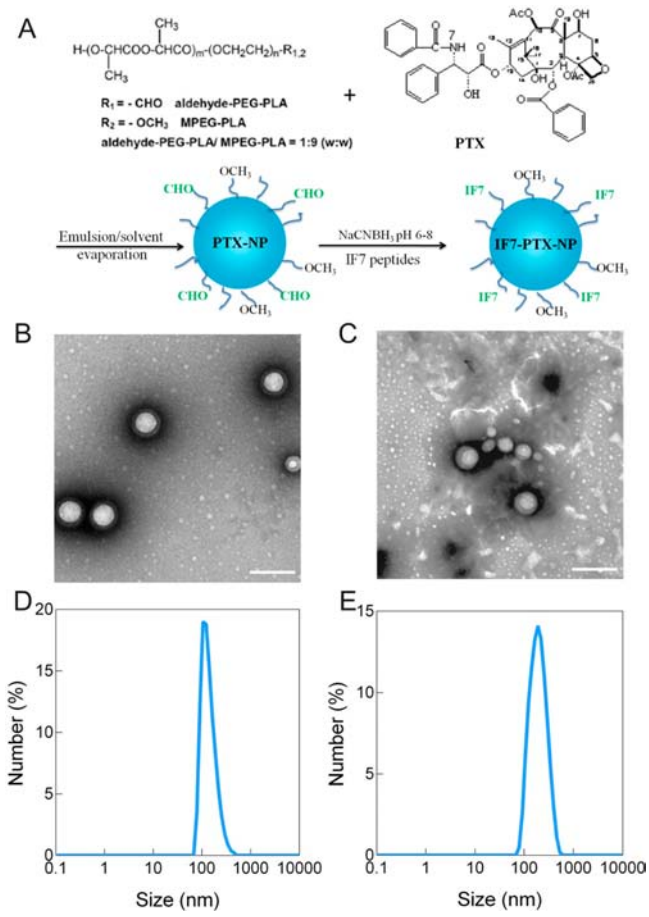

Figure 1. (A) Schematic diagram of IF7-PTX-NP preparation. TEM photographs of IF7-PTX-NP (B) and PTX-NP (C), bar, 200 nm. Particle size and size distribution of IF7-PTX-NP (D) and PTX-NP (E).

PTX-NP (−22.33 ± 2.08 mV), which may be due to the conversion of the free −CHO groups. IF7-PTX-NP and PTX-NP did not differ markedly in their encapsulation efficiency or drug loading, suggesting that no significant amount of PTX leaked during the conjugation of PTX-NP with IF7. Each IF7-PTX-NP particle had an average of 1227 ± 109 peptides on its surface, and the mean distance between neighboring PEG chains linked to the peptides was 8.71 ± 0.37 nm, forming a multivalent ligand decoration.

In Vitro Release and in Vivo Pharmacokinetic Study. As shown in Figure 2A, PTX was released in a biphasic pattern: initial rapid release was followed by slower sustained release in PBS (pH 4.0 and pH 7.4). In medium containing 50% rat plasma (Figure 2B), PTX was released from IF7-PTX-NP at a constant rate after burst release for 30 min. The drug release from both types of nanoparticles was much faster in an environment containing plasma than in PBS (at both pH 4.0 and pH 7.4). This may be the result of increased drug diffusion induced by the plasma enzyme-catalyzed hydrolysis of the polymer matrix. No significant difference was observed in the drug release from IF7-PTX-NP and PTX-NP in PBS at pH 7.4 or pH 4.0 and in rat plasma ($P > 0.05$).

The blood clearance curves for PTX loaded in nanoparticles after their intravenous administration to Sprague−Dawley rats are shown in Figure 2C and Table 2. IF7-PTX-NP and PTX-NP showed high initial blood circulation levels compared with

DOI: 10.1021/acs.bioconjchem.5b00283
Bioconjugate Chem. 2015, 26, 1702−1712

Table 1. Physicochemical Characteristics of Nanoparticles Modified with and without IF7 Peptide

	particle size (nm)							
nanoparticles	DLS[a]	TEM[b]	zeta potential (mV)	DL[c] (%)	EE[d] (%)	CE[e] (%)	S^f	d^g (nm)
PTX-NP	143.20 ± 13.27	83.57 ± 6.80	−22.33 ± 2.08	10.46 ± 3.15	51.80 ± 3.38	-	-	-
IF7-PTX-NP	156.43 ± 25.41	92.68 ± 8.68	−15.67 ± 1.53	7.22 ± 0.75	46.77 ± 1.22	9.48 ± 0.82	1227 ± 109	8.71 ± 0.37

[a]Mean hydrodynamic diameter determined by DLS. [b]Particle size measured by TEM (n = 10). [c]Drug loading. [d]Encapsulation efficiency. [e]Conjugation efficiency. [f]IF7 surface deansity. [g]Mean distance between two neighboring PEG chains which linked to the IF7 peptide.

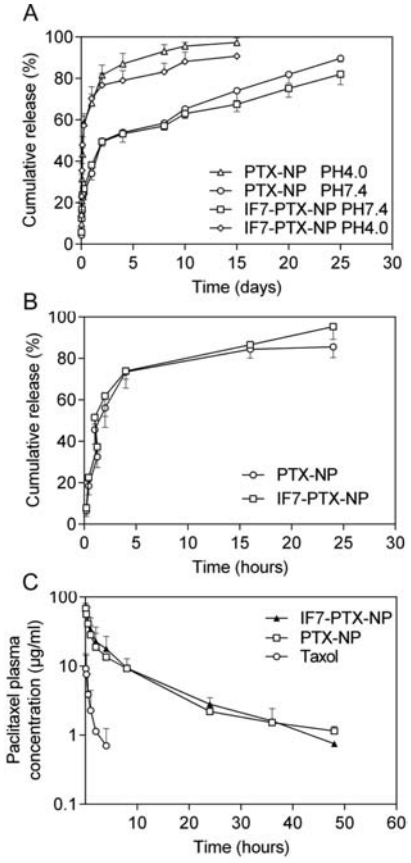

Figure 2. (A) In vitro release profile of paclitaxel from nanoparticles in PBS (pH 7.4 and 4.0). (B) In vitro release profile of paclitaxel in the mixture medium (1:1, v/v) of PBS (pH 7.4) and rat plasma. (C) Concentration−time profiles of paclitaxel in plasma after i.v. administration of paclitaxel injection (Taxol), PTX-NP, and IF7-PTX-NP, respectively (n = 7). Values expressed as means ± SD.

Table 2. Pharmacokinetic Parameters of Taxol, PTX-NP, and IF7-PTX-NP

parameters	taxol	PTX-NP	IF7-PTX-NP
$T_{1/2}$ (h)	1.58 ± 0.71	14.04 ± 4.87*	12.31 ± 1.93*
AUC(h · μg/mL)	5.79 ± 3.00	160.28 ± 46.42*	229.95 ± 74.81*
CL (mL/h)	149.71 ± 81.88	4.75 ± 2.00	4.61 ± 1.84

*P < 0.001 as compared with Taxol.

Taxol, whereas PTX formulated as Taxol was quickly removed from the circulation, by 4 h after administration. In contrast, IF7-PTX-NP and PTX-NP displayed markedly delayed blood clearance. The pharmacokinetic parameters determined with a statistical moments analysis showed that PTX-NP and IF7-PTX-NP extended the half-life of Taxol from 1.58 ± 0.71 h to 14.04 ± 4.87 h and 12.31 ± 1.93 h, respectively. The area under the concentration−time curve (AUC) increased about 40-fold for IF7-PTX-NP and 28-fold for PTX-NP compared with that for Taxol, whereas there was no significant difference in the AUCs of IF7-PTX-NP and PTX-NP (P > 0.05). These results suggested that modification with the IF7 peptide did not influence the in vivo long-circulating properties of the nanoparticles.

IF7 Conjugation Mediates Active Nanoparticle Internalization by Human Umbilical Vein Endothelial Cells (HUVEC). The uptake and internalization of coumarin 6-labeled nanoparticles by HUVEC were examined with confocal laser scanning microscopy (CLSM) (Figure 3). The nonspecific uptake of coumarin 6-labeled unmodified nanoparticles (coumarin 6-labeled NP) was observed, but more coumarin 6-labeled IF7-modified nanoparticles (coumarin 6-labeled IF7-NP) were internalized (P < 0.001), evident as a ~40% increase in the fluorescence intensity in the cells (Figure 3B). This suggested that the IF7 decoration on the particle surface

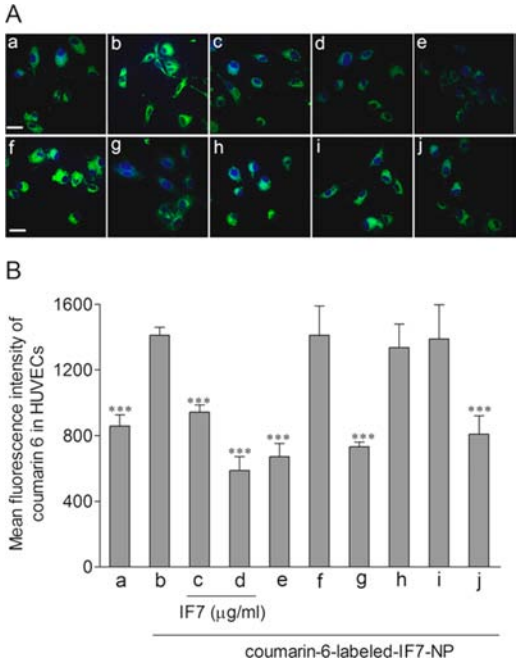

Figure 3. Internalization of coumarin 6-labeled IF7-NP into HUVEC. (A) Representative confocal laser scanning micrographs of HUVEC after 2 h culture with coumarin 6-labeled NP (a), coumarin 6-labeled IF7-NP (b), or preincubation with 1 μg/mL (c), or 5 μg/mL (d) free IF7 peptide or coumarin 6-labeled IF7-NP at 4 °C (e), 3 μM cytochalasin D (f), 10 μM filipin (g), 10 μM nystatin (h), 10 μM chlorpromazine (i), 30 μM phenylarsine oxide (j) for 30 min before the cells were exposed to coumarin 6-labeled IF7-NP for 2 h at 37 °C. The green shows the nanoparticles inside the cells and the blue shows the cell nuclei. Bar, 20 μm. (B) Quantitation of mean fluorescence intensity of coumarin 6 in HUVECs. Values are from 6 to 8 individual cells and expressed as means ± SD. ***P < 0.001 as compared with coumarin 6-labeled IF7-NP.

DOI: 10.1021/acs.bioconjchem.5b00283
Bioconjugate Chem. 2015, 26, 1702−1712

significantly facilitated the uptake of the nanoparticles by HUVEC. The uptake of the IF7-NP was dose-dependently inhibited by free IF7, and was lower than the nonspecific uptake of unmodified nanoparticles, confirming that the uptake of IF7-conjugated nanoparticles was mainly mediated by the interaction between IF7 and Anxa l specifically overexpressed on the HUVEC surface.

The internalization of coumarin 6-labeled IF7-NP into HUVEC was also significantly inhibited at 4 °C, in the presence of phenylarsine oxide and filipin, indicating that ATP consumption and caveolae are involved in the uptake process. Cytochalasin D, chlorpromazine, and nystatin did not attenuate the uptake of IF7-NP, suggesting that macropinocytosis, clathrin, and lipid raft are not involved in the endocytosis process.

Assays of HUVEC Viability, Migration, and Tube Formation. HUVEC cells are classical in vitro model with properties resembling tumor vascular ECs. IF7-PTX-NP was significantly more cytotoxic to HUVEC than Taxol at concentrations from 1 pM to 1 nM, and than PTX-NP at concentrations from 0.1 pM to 1 nM (Figure 4A). Neither the blank NP nor IF7-NP influenced the viability of HUVEC, indicating that the PEG−PLA polymer is not cytotoxic and that the IF7 linked to the particles is not directly toxic to HUVEC.

Compared with Taxol, IF7-PTX-NP exhibited overall significantly greater activity in inhibiting HUVEC migration (Figure 4B,C−F) and tube formation (Figure 4G,H−K) at the tested concentrations. IF7-PTX-NP caused dramatically higher HUVEC migration inhibition than PTX-NP at 1 pM, and tube formation inhibition than PTX-NP from 1 pM to 0.1 nM. Although nontoxic to HUVEC, the unloaded nanoparticles and especially IF7-NP displayed moderate abilities to inhibit HUVEC migration and tube formation, indicating that the IF7 decoration on the particle surface maintained its endogenous antiangiogenic activity, although at much lower levels than the activity of the model drug PTX.

In Vivo Angiogenesis in the Matrigel Plug Assay in Mice. As shown in Figure 5, IF7-PTX-NP significantly inhibited neovascularization in the Matrigel plug compared with the control (saline), whereas PTX-NP at the same dose did not effectively reduce the number of blood vessels. The effect of IF7-conjugated PTX-NP on in vivo angiogenesis in the Matrigel plugs was effectively blocked by free IF7 peptide.

In Vivo Tumor Targeting and Biodistribution. DiR-labeled IF7-NP accumulated dramatically more in the MCF-7/ADR tumor tissues than DiR-labeled NP only 1 h after injection, and this pattern was maintained for the entire study (72 h after injection; Figure 6A). Ex vivo imaging confirmed that IF7 conjugation led to much greater accumulation of the nanoparticles in the tumors (Figure 6B,C). The tumor-targeted accumulation of IF7-conjugated nanoparticles in vivo was efficiently blocked by free IF7 peptide, indicating the dominant contribution of IF7 to the targeting of the nanoparticles to the tumor. Free DiR did not accumulate significantly in the tumors. Therefore, the tumor targeting and accumulation of IF7-PTX-NP might be attributed to both the PEG "corona", which confers the long-circulation property on IF7-PTX-NP, and the IF7 peptide, which endows the nanoparticles with their active targeting ability. Besides the tumors, the nanoparticles were also distributed in the reticuloendothelial system, including in the lung, liver, and spleen.

Tumor Vessel Targeting in Vivo. The immunofluorescence results indicated that coumarin 6-labeled IF7-PTX-NP

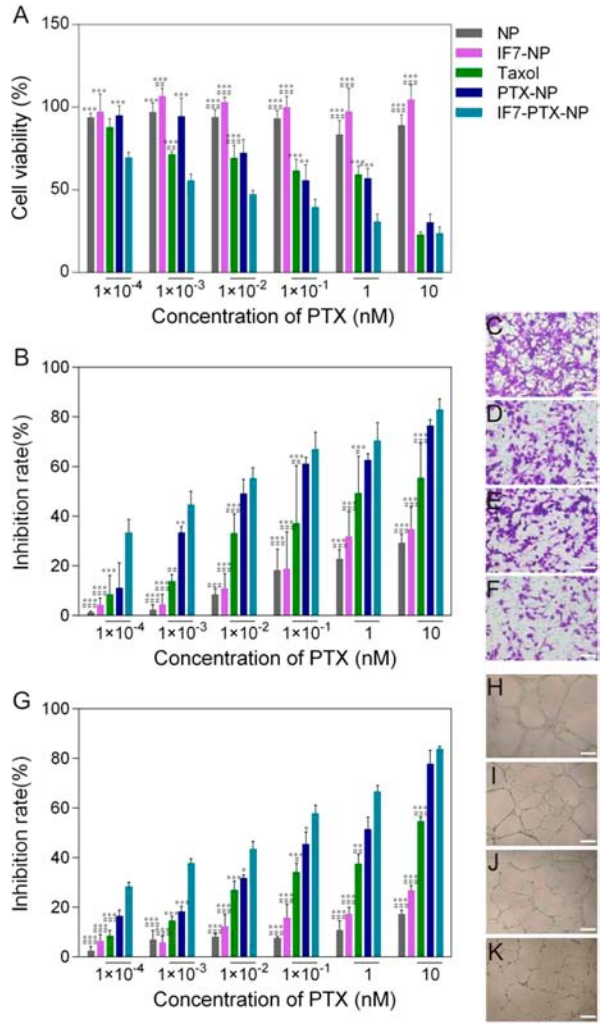

Figure 4. IF7 conjugation improves nanoparticles' activity in inhibiting HUVEC viability, migration, and tube formation. (A) Cell viability was evaluated after 48 h treatment. (B−F) HUVEC migration after 8 h treatment was assayed using the Transwell Boyden chamber. The migrated cells were visualized by staining with crystal violet, and quantified using colorimetry after extracting the dye with acetic acid. (G−K) Tube formation after 10 h treatment was examined using Chemicon In Vitro Angiogenesis Assay Kit. The representative photographs of HUVEC migration (C−F) and tube formation (H−K) after treatment with various PTX formations at 0.1 nM were shown. C,H: control; D,I: Taxol; E,J: PTX-NP; F,K: IF7-PTX-NP. Bar, 200 μm. For blank NP and IF7-NP, the nanoparticle concentration was adjusted to be the same in all cases with nanoparticle involved. Values are expressed as mean ± SD, n = 5−6. $^{*}P < 0.05$, $^{**}P < 0.01$, $^{***}P < 0.001$ as compared with IF7-PTX-NP, $^{\#}P < 0.05$, $^{\#\#}P < 0.01$, $^{\#\#\#}P < 0.001$ as compared with PTX-NP.

specifically targeted the tumor vessels and induced apoptosis in ECs, appearing as a white signal, arising from the merging of the green (coumarin 6), blue (CD31), and red signals (TUNEL) (Figure 7A2), and also led to the dramatic necrosis of the tumor tissues (Figure 7B2). In contrast, the nonspecific homing to the tumor neovasculature of the nonconjugated nanoparticles was very weak (Figure 7A1, B1). An inhibition test with excessive free peptide confirmed the EC-targeting property of the IF7-conjugated nanoparticles (Figure 7A3, B3).

Antitumor Effect in Resistant MCF-7/ADR Xenografts. The tumor growth curves are shown as different combinations of the various groups for comparison in Figure 8A−C.

DOI: 10.1021/acs.bioconjchem.5b00283
Bioconjugate Chem. 2015, 26, 1702−1712

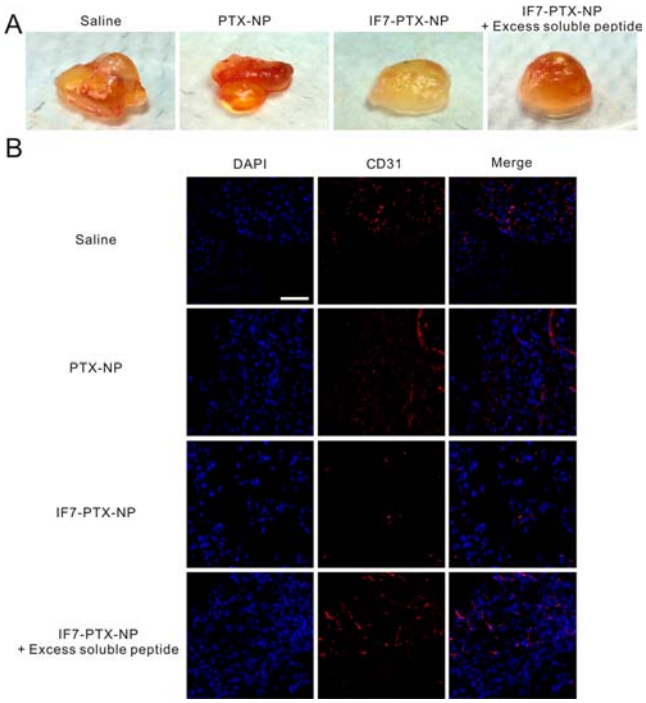

Figure 5. IF7-PTX-NP treatment leads to enhanced antiangiogenesis efficacy in Matrigel plugs. Female BALB/c nude mice were injected subcutaneously with growth factor-reduced Matrigel containing human recombinant bFGF. Three doses (day 2, 4, 6) at 2.5 mg/kg PTX were administered through the caudal vein to the mice, respectively, and the mice were sacrificed at day 7 for the examination of the Matrigel plugs. n = 3 in each group. (A) Photographs of Matrigel plugs of different groups at day 7. (B) CD31 staining sections showing the vessel in each Matrigel plug. Bar, 50 μm.

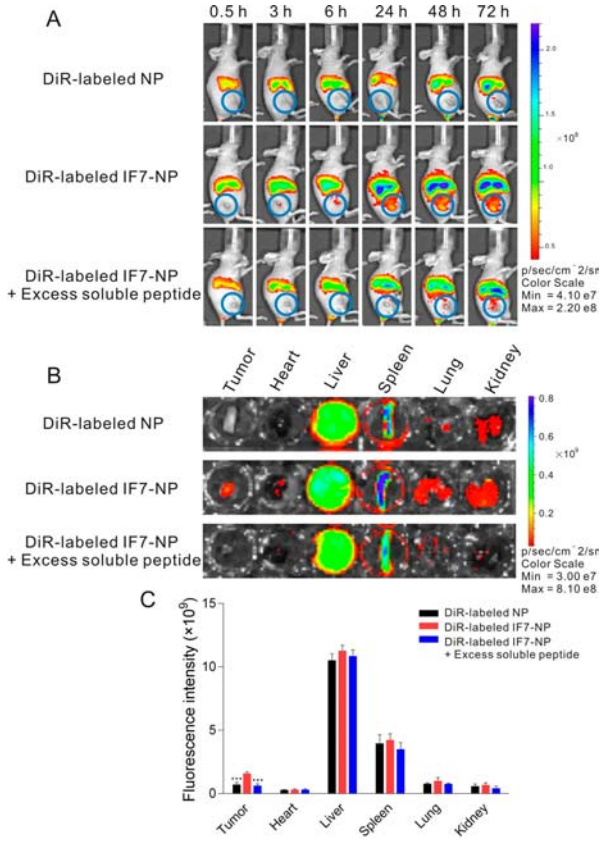

Figure 6. IF7 conjugation facilitates nanoparticle accumulation in tumors. (A) Female BALB/c mice bearing MCF-7/ADR tumor (~100 mm^3) were given a single intravenous injection of DiR-labeled NP or IF7-NP at DiR dose of 0.1 mg/kg, or coinjection of DiR-labeled IF7-NP and excess free IF7. At 0.5, 3, 6, 24, 48, and 72 h after injection, mice with in vivo DiR fluorescence were imaged in Xenogen IVIS 200 system. The tumor location was indicated with blue circles. (B) At 72 h after injection, the mice were sacrificed, and tumors and major organs and tissues were harvested and placed in the 24-well plate for ex vivo imaging. (C) Quantitative DiR fluorescence intensity in tumor and other organs at 72 h after injection of DiR-labeled nanoparticles. Values are expressed as mean ± SD, n = 4. ***P < 0.001 as compared with DiR-labeled IF7-NP.

Compared with the control (saline), IF7-PTX-NP treatment with a low dose of paclitaxel (1 mg/kg) dramatically inhibited tumor growth, whereas Taxol and PTX-NP at the same dose did not effectively delay tumor growth (Figure 8A). Increasing the dose of paclitaxel, administered as Taxol, to a high level (8 mg/kg) still did not retard tumor growth, but the involvement of XR9576 (a strong P-gp inhibitor) with a high dose of Taxol (8 mg/kg), but not a low dose (1 mg/kg), significantly inhibited tumor progression, resulting in an anticancer efficacy similar to that of IF7-PTX-NP (1 mg/kg) (Figure 8B). The anticancer effect of IF7-PTX-NP (1 mg/kg) was not influenced by the involvement of XR9576, but was dramatically blocked by the coadministration of an excess of free IF7 peptide (Figure 8C), suggesting that the antiangiogenic role of the tumor-vessel-targeting nano-DDS was the dominant factor in the treatment of resistant MCF-7/ADR cancer. No significant differences were observed in the mouse bodyweights before and after the various treatments (Figure 8D).

To further determine whether the improved antitumor efficacy was related to the enhanced antiangiogenic activity, immunohistochemical assays of the tumor tissues were performed. Compared with the control group (Saline), all other treatments (except Taxol 1 mg/kg and Taxol 1 mg/kg + XR9576) significantly reduced microvessel density (MVD) in the tumors, and IF7-PTX-NP caused the greatest reduction in tumor MVD, which was dramatically blocked by free IF7 (Figure 9A and B). IF7-PTX-NP also caused more apoptosis of tumor cells than the other treatments, except those involving Taxol (8 mg/kg) + XR9576. Free IF7 clearly blocked the apoptosis-inducing effect of IF7-PTX-NP on tumor cells (Figure 9 C and D).

■ DISCUSSION

Angiogenesis, the development of new vessels from the existing vasculature, plays a central role in tumor growth, survival, and progression. The inhibition of tumor angiogenesis can slow or halt tumor growth, or even cause tumors to regress. In this study, we developed IF7-peptide-conjugated nanoparticles (IF7-NP) that can specifically deliver antiangiogenic molecules to the ECs of the tumor neovasculature as an antiangiogenic cancer therapy. Paclitaxel, a representative cytotoxic drug with potent antiangiogenic activity,[18,19] was selected as the prototype drug in this study.

After oil/water emulsion and solvent evaporation, the aldehyde groups of the polymer protruded from the nanoparticle surface. IF7 was then conjugated to the aldehyde groups via its α-amino group in the presence of $NaCNBH_3$ to generate IF7-PTX-NP (Figure 1A). In this process, we utilized the technique of N-terminal PEGylation, a method that has been successfully used in one commercial product, Neulasta, a

DOI: 10.1021/acs.bioconjchem.5b00283
Bioconjugate Chem. 2015, 26, 1702−1712

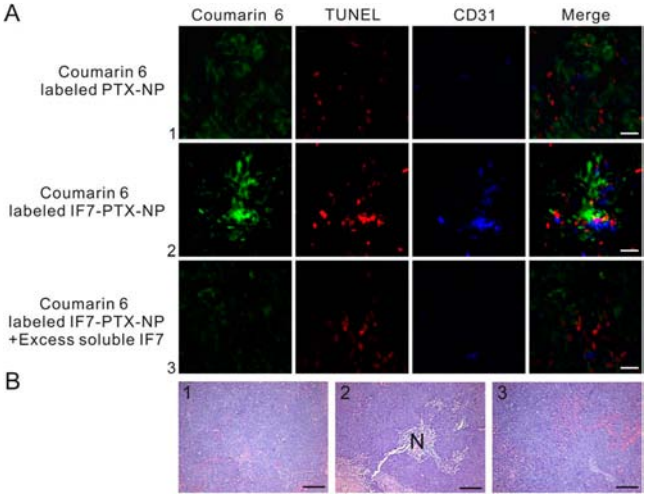

Figure 7. IF7 conjugation achieves nanoparticle targeting to tumor vessel. (A) Female nude mice bearing MCF-7/ADR tumor were intravenously administered with coumarin 6-labeled PTX-NP or IF7-PTX-NP at PTX dose of 2.5 mg/kg, or coumarin 6-labeled IF7-PTX-NP plus excess free IF7. After 48 h, the mice were sacrificed, and the tumors were resected, sectioned, and stained for CD31 (endothelial cells) (blue, pseudo color) and TUNEL (apoptosis, red). Bar, 50 μm. (B) Hematoxylin and eosin staining (H&E) and pathological analysis of tumors. N, Necrosis tissues. Bar, 100 μm. Compared with coumarin 6-labeled PTX-NP (A1, B1), delivery of PTX by coumarin 6-labeled IF7-PTX-NP to tumor neovasculature induced significant apoptosis of endothelial cells and necrosis of tumor tissues (A2, B2), and this phenomenon can be effectively hindered by 50-fold molar excess IF7 peptide (A3, B3).

drug used to treat granulocyte depletion during chemotherapy.[21] This selective N-terminal attachment of a functional ligand to the PEG chain could achieve discrete, single-position PEGylation and usually preserve the conformation and biological activity of the attached protein or peptide.[22] After optimizing the main process parameters for IF7-PTX-NP with respect to its encapsulation efficiency and drug loading, the amount of IF7 linked to the particle surface was determined with a rapid and highly sensitive 3-(4-carboxybenzoyl)-quinoline-2-carboxaldehyde (CBQCA)-based fluorescence method.[23] The multivalent array of IF7 ligands on the surfaces of the nanoparticles offered stronger binding efficacy to Anxa 1, with multivalent linking to the targeted cells, and facilitated the ligand−receptor-mediated internalization of the nanoparticles.

Decoration with the IF7 peptide did not change the release rate of the nanoparticles in vitro (Figure 2A,B). The release of PTX from IF-PTX-NP and PTX-NP persisted for 25 days in PBS and 24 h in 50% plasma. The superiority of IF7-PTX-NP compared with Taxol is attributed to both the IF7 peptide and the PEG corona. The PEG corona endows the nanoparticles with a "stealth" property, extends the circulation time (Figure 2C), and thus increases the probability of binding to the Anxa 1 receptors on ECs in the tumor neovasculature. Paclitaxel formulated as Taxol was quickly eliminated from the blood compartment, so only a very small amount of PTX reached the ECs of the tumor neovasculature. Therefore, to achieve an antiangiogenic effect in vivo, lower doses of PTX formulated in IF7-PTX-NP can be used than when it is formulated as Taxol, and fewer concomitant adverse effects could be expected.

The facilitated internalization of IF7-labeled NP into HUVEC through the IF7 ligand was visualized in the uptake

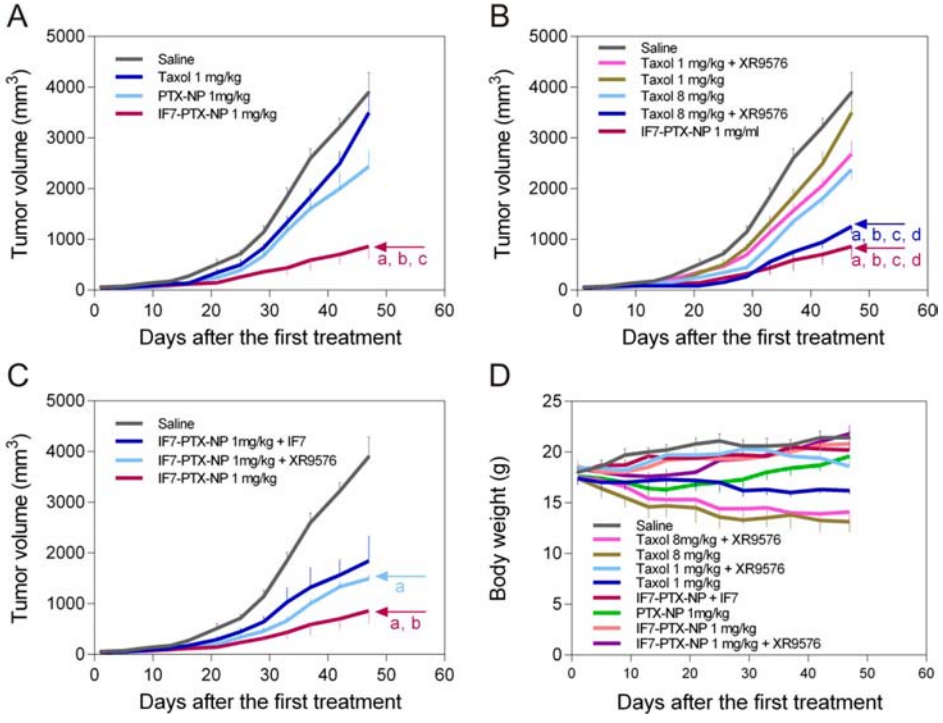

Figure 8. IF7-PTX-NP results in enhanced antitumor efficacy in the MCF-7/ADR xenografts in female nude mice. For the sake of comparison, the tumor growth curves were shown in different combinations of the various groups. Tumor volumes are represented as Mean ± SEM of five mice in each group. (A) a, $P < 0.05$ vs Saline; b, $P < 0.05$ vs Taxol (1 mg/kg); c, $P < 0.05$ vs PTX-NP (1 mg/kg); (B) a, $P < 0.05$ vs Saline; b, $P < 0.05$ vs Taxol (1 mg/kg); c, $P < 0.05$ vs Taxol (1 mg/kg) + XR9576; d, $P < 0.05$ vs Taxol (8 mg/kg); (C) a, $P < 0.05$ vs Saline; b, $P < 0.05$ vs IF7-PTX-NP (1 mg/kg) + IF7. D. Body weight variations of the mice after various treatments. Data are presented as Mean ± SEM ($n = 5$).

DOI: 10.1021/acs.bioconjchem.5b00283
Bioconjugate Chem. 2015, 26, 1702−1712

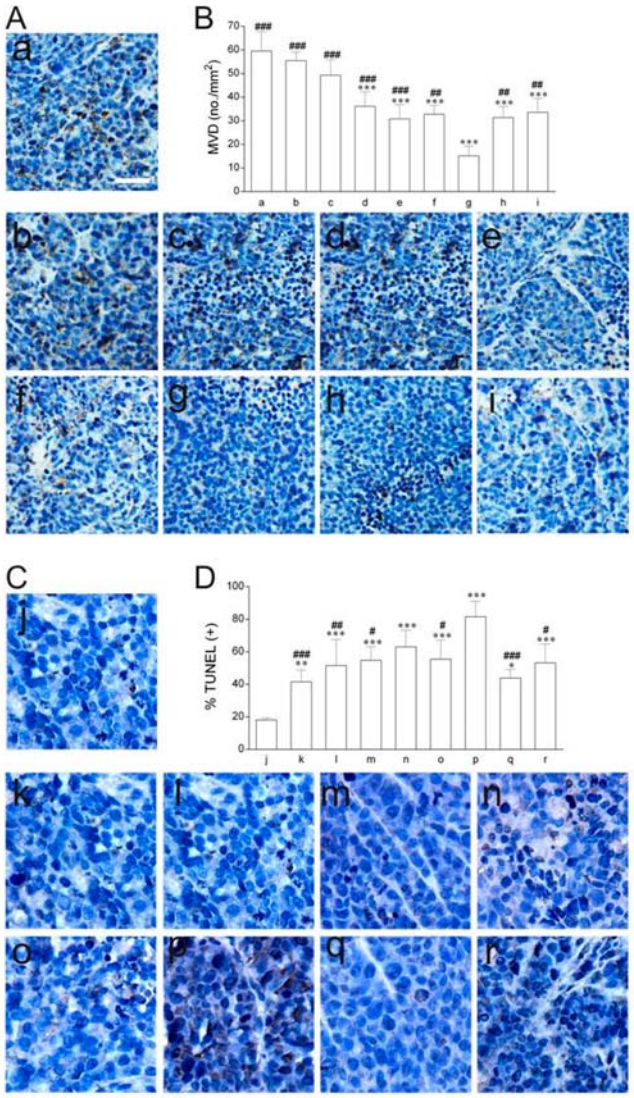

Figure 9. Immunohistochemistry assay of mouse microvessel density (MVD) (A,B) and tumor cell apoptosis (C,D) in MCF-7/ADR xenografts after various treatments. The brown color indicates the positive staining of microvessel (A) or the apoptotic cells (C). Saline (a, j); Taxol 1 mg/kg (b, k); Taxol 1 mg/kg + XR9576 (c, l); Taxol 8 mg/kg (d, m); Taxol 8 mg/kg + XR9576 (e, n); PTX-NP (f, o); IF7-PTX-NP 1 mg/kg (g, p); IF7-PTX-NP 1 mg/kg + IF7 (h, q); IF7-PTX-NP 1 mg/kg + XR9576 (i, r). $^{*}P < 0.05$, $^{**}P < 0.01$, $^{***}P < 0.001$ as compared with the Saline; $^{\#}P < 0.05$, $^{\#\#}P < 0.05$, $^{\#\#}P < 0.01$, $^{\#\#\#}P < 0.001$ as compared with IF7-PTX-NP (1 mg/kg).

experiment (Figure 3). The improved uptake led to their anticipated enhanced antiangiogenic activity. IF7 targeting led to the dramatically enhanced antiangiogenic activity of IF7-PTX-NP compared with that of PTX-NP (Figure 4). It must be noted that the inhibition of HUVEC angiogenesis by various PTX formulations was not attributable to the direct cytotoxicity of PTX, because at the given drug concentrations and exposure times, HUVEC proliferation was not affected (data not shown). The enhanced antiangiogenic properties of IF7-PTX-NP could be ascribed to their active internalization, mediated by the interaction between IF7 and Anxa 1, which is specifically highly expressed on ECs. It is also noteworthy that the multivalent IF7 attached to the particle surface confers on the nanoparticles a high affinity for ECs. To evaluate the in vivo antiangiogenic effect, we performed a Matrigel plug assay in mice (Figure 5). IF7-PTX-NP successfully inhibited neovascularization, and its antiangiogenic activity was effectively blocked by free IF7 peptide, indicating the dominant contribution of the peptide to the vessel targeting by the nanoparticles.

A multidrug-resistant cancer model was established using MCF-7/ADR cells, a human breast cancer cell line with inherent P-gp expression. MCF-7/ADR cells have a moderate MDR phenotype, which makes them more suitable as an MDR model for preclinical studies than other cell lines deliberately developed to have unusually high resistance.[24−26] P-gp is one of the MDR-related proteins and is encoded by the multidrug resistance 1 gene (*MDR1*). P-gp is also the main type of drug-resistance protein in MCF-7/ADR cells.[27,28] Verapamil and XR9576 (tariquidar) represents first- and third-generation P-gp inhibitors, respectively. The involvement of these two inhibitors dramatically reduced the IC_{50} values of various PTX formulations in HCT-15 cells, indicating a P-gp-mediated resistant phenotype.[29] XR9576 is more potent than verapamilin in sensitizing MCF-7/ADR to Taxol and the other two paclitaxel-loaded nanoparticles.[30] In view of its better performance and safety in the clinical context, XR9576 was chosen rather than verapamil for the in vivo animal experiment in this study.[31,32]

The targeting of tumor vessels by IF7-PTX-NP increased the nanoparticle accumulation in the MCF-7/ADR resistant breast tumors. Most importantly, the targeted antiangiogenic effect of IF7-PTX-NP induced significant apoptosis in the MCF-7/ADR tumor vascular ECs and necrosis of the tumor tissues. When the therapeutic target was shifted from the resistant tumor cells to the sensitive tumor vascular ECs, a low dose of PTX formulated in IF7-PTX-NP (1 mg/kg) exerted a significant anticancer effect, inhibiting the growth of the resistant MCF-7/ADR tumors to an extent only achieved with an 8-fold higher dose PTX (8 mg/kg) as Taxol plus XR9576. The inhibition test using free IF7 indicated that the anticancer effect of IF7-PTX-NP was mainly derived from their tumor-vessel-targeting and antiangiogenic activities, and not from the direct toxic effect on the resistant tumor cells. The mouse body weights were maintained well throughout the anticancer test, implicating the lower toxicity of the targeted antiangiogenic chemotherapy in the animals. The immunohistochemical assays demonstrated that the anticancer efficacy of IF7-PTX-NP was related to its improved antiangiogenic effect, evident in the dramatically reduced MVD and pronouncedly increased numbers of apoptotic tumor cells.

■ CONCLUSIONS

In this study, we developed a nano-DDS decorated with the IF7 peptide as the targeting ligand for tumor-neovasculature-targeted drug delivery. The IF7-Anxa 1-mediated recognition of and internalization by ECs significantly facilitated the uptake of the IF7-conjugated nanoparticles by ECs, and IF7-PTX-NP displayed significantly stronger in vitro antiangiogenic activity than Taxol or PTX-NP, as shown by its effects on HUVEC proliferation, migration, and tube formation.

When human breast cancer MCF-7/ADR cells were used as the drug-resistant tumor model, the long-circulation property and the IF7 ligand of IF7-PTX-NP allowed the rapid, long-term, and accurate targeting of the tumor neovasculature in vivo, and more importantly, induced significant apoptosis of the tumor vascular ECs and necrosis of the tumor tissues. These findings clearly show that targeting the neovasculature with PTX in nanoparticles has similar anticancer efficacy as an 8-fold

DOI: 10.1021/acs.bioconjchem.5b00283
Bioconjugate Chem. 2015, 26, 1702−1712

higher dose of PTX formulated as Taxol plus XR9576. These results provide a promising basis for the further investigation of targeted antiangiogenic chemotherapy for resistant cancers.

EXPERIMENTAL PROCEDURES

Materials, Cell Culture, and Animals. Aldehyde poly(ethylene glycol)-poly(lactide) (CHO-PEG-PLA; MW, 64 kDa) and methoxy poly(ethylene glycol) (CH_3O-PEG-PLA (MW, 61 kDa) block copolymers were synthesized with the ring-opening polymerization method in our laboratory.[22] The IF7 peptide (IFLLWQR) was synthesized by GL Biochem (Shanghai, China). PTX was supplied by Knowshine Pharmachemicals (Shanghai, China). High performance liquid chromatography (HPLC) was used to determine the concentrations of PTX with the Agilent 1100 HPLC System (Agilent, Japan). Docetaxel (DTX, internal standard for HPLC) was supplied by Aladdin Reagent Company (China). Taxol was from Bristol-Myers Squibb Company. Coumarin 6, filipin, chlorpromazine, cytochalasin D, nystatin, and phenylarsine oxide were from Sigma-Aldrich (St. Louis, MO). 1,10-Dioctadecyl-3,3,30,30-tetramethyl indotricarbocyanine iodide (DiR) and the CBQCA Protein Quantitation Kit were from Life Technologies (Carlsbad, CA). phycoerythrin (PE)-Cy5-labeled goat anti-rabbit immunoglobulin G (IgG) antibody were from Santa Cruz Biotechnology (Santa Cruz, CA). Anti-CD31 antibody was from Abcam (Hong Kong). Tariquidar (XR9576), a P-gp efflux inhibitor, was synthesized by UHN Shanghai R&D Co., Ltd. (Shanghai, China). All other chemicals were of analytical grade and used without further purification.

HUVEC and M200 medium were obtained from Life Technologies. HUVEC from passages 3−5 were used in the experiments. The resistant MCF-7/ADR human breast cancer cell line and RMPI 1640 medium were obtained from KeyGEN Biotech Company (Nanjing, China).

Female BALB/c nude mice (20 ± 2 g) and Sprague−Dawley (SD) rats were provided by the Shanghai Laboratory Animal Center (Chinese Academy of Sciences). Care and handling of animals and animal experiments conducted in this study were approved by the appropriate Ethical Committee of Shanghai Jiao Tong University School of Medicine.

Preparation of IF7-PTX-NP. IF7-PTX-NP was fabricated with the emulsion and solvent evaporation method, with subsequent surface functionalization (Figure 1A). Briefly, 6 mg of PTX was dissolved in 1 mL of a solution containing 60 mg of aldehyde-PEG-PLA blended with MPEG-PLA (1:9, w/w) in dichloromethane. Next, 3 mL of 1% (w/v) sodium cholate was slowly poured into the solution and the mixture was sonicated at 240 W for 30 s (Scientz Biotechnology, Ningbo, China). The oil/water emulsion was diluted further with 40 mL of 0.5% (w/v) sodium cholate solution and then gently stirred overnight at room temperature with a magnetic stirrer to evaporate the organic solvent. The resulting PTX-loaded nanoparticles (PTX-NP) were collected by centrifugation (11 000 × *g*, 30 min, 4 °C; Sigma 3K18 centrifuge, Germany) and washed twice to remove excess emulsifier. PTX-NP was then incubated with IF7 peptide in a 1:3 molar ratio, and bound to the aldehyde group at the N-terminal amine of IF7. The conjugation reaction was conducted in PBS (pH 7.4) at room temperature for 10 h in the presence of $NaCNBH_3$, a reducing reagent. The unconjugated IF7 peptide was removed by centrifugation (11 000 × *g*, 30 min, 4 °C) and the IF7-PTX-NP was collected. Coumarin 6- or DiR-labeled nanoparticles were prepared in the same way, except that in the oil phase, PTX was replaced or mixed with 0.3% (w/v) coumarin 6 or 0.2% (w/v) DiR, respectively.

Nanoparticle Characterization. The shape and morphology of the nanoparticles were observed with H-600 TEM (Hitachi, Japan). The particle size and zeta potential were determined with DLS using a NiComp 380 ZLS instrument (Particle Sizing Systems, Santa Barbara, CA). The encapsulation efficiency and drug loading were determined as previously described.[22] The IF7 conjugation efficiency was determined by estimating the amount of nanoparticle-associated peptide with the CBQCA Protein Quantitation Kit.[33] The peptide density on nanoparticle surface and the distance between neighboring PEG chains were determined according to the methods we previously reported.[22]

In Vitro Release Study. Experiments to evaluate the release of PTX from the nanoparticles in vitro were performed at different pH at 37 °C to determine whether pH affects the release rate. Briefly, 3 mg of IF7-PTX-NP or PTX-NP was placed in a centrifuge tube and suspended in 10 mL of PBS (pH 7.4 or 4.0) containing 0.1% Tween 80 to maintain the sink condition. The tubes were placed in a gas bath at 37 °C with shaking at 100 rpm. At specific intervals, the nanoparticles were centrifuged (11 000 × *g*, 30 min, 4 °C). The release medium containing the free drug was removed and another 10 mL of fresh PBS was added to the test tubes to resuspend the particles for the continuous release study. The supernatant containing the drug was extracted with dichloromethane and analyzed with HPLC. Each measurement was made in triplicate.

The release of the nanoparticles in vitro was also evaluated in medium containing rat plasma to determine whether the release rate was altered by plasma. Typically, 3 mg of nanoparticles was placed in a centrifuge tube and incubated with a mixture of PBS (pH 7.4) and plasma (1:1, v/v) containing 0.01% NaN_3. The tubes were placed in a gas bath at 37 °C with shaking at 100 rpm. At specific intervals, the nanoparticles were separated by centrifugation (11 000 × *g*, 30 min, 4 °C) and the supernatant containing the drug was analyzed with HPLC. Each measurement was made in triplicate.

In Vivo Pharmacokinetic Study. Female Sprague−Dawley rats weighting 200 ± 20 g were used in the pharmacokinetic study. Taxol, PTX-NP, and IF7-PTX-NP were diluted to the required concentrations in physiological saline solution (0.9%, w/v) before administration. Each animal was treated intravenously through the caudal vein with 6 mg/kg of paclitaxel. At 5, 10, and 30 min, and 1, 2, 4, 8, 24, 36, and 48 h after the drug was administered, blood samples (0.25 mL) were collected from the orbital veins.

The paclitaxel plasma concentration was analyzed according to a previously reported method.[22] Briefly, 100 μL of each plasma sample was mixed with 2 mL of *tert*-butyl methyl ether and 5 μL of 2 mg/mL docetaxel in methanol as the internal standard. The mixture was stirred for 30 s and then centrifuged at 2500 × *g* for 20 min. The supernatant was transferred to a clean tube and dried under nitrogen. The residue was reconstituted with 100 μL of the mobile phase composed of acetonitrile and water (60:40, v/v) and then subjected to HPLC with detection at 227 nm. The flow rate of the mobile phase was 1.0 mL/min and the column temperature was 25 °C. The pharmacokinetic parameters were calculated with the Phoenix *WinNonlin* software (version 6.1; Pharsight Corporation).

Internalization Mechanism of IF7-Conjugated Nanoparticles. To examine the cellular uptake of the IF7-

DOI: 10.1021/acs.bioconjchem.5b00283
Bioconjugate Chem. 2015, 26, 1702−1712

conjugated nanoparticles, HUVEC were cultured on VWR Micro Cover Glasses (VWR International, Radnor, PA) in 24-well plates at a density of 5×10^4 cells/well. When the cells reached about 80% confluence, the medium was replaced with 30 μg/mL coumarin 6-labeled nanoparticles (coumarin 6-NP) or coumarin 6-labeled IF7-conjugated nanoparticles (coumarin 6-labeled IF7-NP) in medium and incubated for 30 min. After the nanoparticles were removed and the wells washed twice with PBS, the cells were fixed with 4% glutaraldehyde for 20 min, and the cell nuclei were stained with Hoechst 33342 for 30 s. The cells were then observed under an LSM-510 CLSM (Carl Zeiss AG, Oberkochen, Germany) with a fluorescein isothiocyanate (FITC) filter (excitation, 488 nm; emission, 520 nm).

To investigate the internalization mechanism, the uptake experiments were performed at low temperature (4 °C) or in the presence of soluble IF7 (1, or 5 μg/mL), filipin (10 μM, to inhibit caveolae-mediated endocytosis), cytochalasin D (3 μM, to inhibit macropinocytosis), chlorpromazine (30 μM, to inhibit clathrin-mediated endocytosis), phenylarsine oxide (30 μM, to deplete ATP), or nystatin (10 μM, to inhibit lipid raft-mediated endocytosis). The HUVEC were incubated with the inhibitors for 30 min before they were incubated with the nanoparticles. The coumarin 6 fluorescence in the HUVEC was quantitated with the Zeiss LSM Image Examiner software (Carl Zeiss MicroImaging, Germany).

Assays of HUVEC Viability, Migration, and Tube Formation. HUVEC viability, migration, and tube formation after treatment with various PTX formulations at drug concentrations of 10^{-4}−10 nM were assayed, as previously described.[22] HUVEC viability after treatment for 48 h was determined using the Cell Counting Kit-8 (Dojindo Laboratories, Kumamoto, Japan). After treatment for 8 h, a HUVEC migration assay was performed in 24-well Transwell Boyden chambers using polycarbonate filters with an 8 μm pore size (Corning, Tewksbury, MA). HUVEC tube formation was evaluated after treatment for 10 h using the In Vitro Angiogenesis Assay Kit (Merck Millipore, Billerica, MA). In all experiments, the same concentrations of blank NP and IF7-NP were also tested as the controls.

In Vivo Angiogenesis in Matrigel Plug Assay in Mice. BALB/c nude mice were injected subcutaneously with 400 μL of growth factor-reduced Matrigel (BD Biosciences) containing 400 ng of human recombinant basic fibroblast growth factor (ProSpec). On days 2, 4, and 6, the mice were injected via the caudal vein with PTX-NP conjugated with or without the IF7 peptide at a PTX dose of 2.5 mg/kg. The blocking effect of a 50-fold molar excess of IF7 on the Matrigel plug was also evaluated. Mice in the control group were injected with saline. On day 7, the mice were killed, and the Matrigel plugs were removed and photographed with a high-resolution digital camera (Canon). Cryostat sections (8 μm) of the plugs were then prepared. The vasculature was stained with rabbit anti-mouse antibody directed against CD31 (1:200) and Alexa-Fluor-647-labeled donkey anti-rabbit IgG (H + L) antibody (1:200). The slides were observed under a Leica TCS SP8 CLSM with far-red filters (Alexa Fluor 647: excitation, 641 nm; long-pass [LP] emission, 668 nm).

In Vivo Imaging and Biodistribution. The real-time distribution and tumor accumulation of DiR-labeled IF7-NP in BALB/c mice bearing MCF-7/ADR xenografts (w100 mm^3) on the right hind limb were monitored under the noninvasive Xenogen IVIS 200 optical imaging system (Caliper Life Sciences, MA). The mice were injected through the caudal vein with 0.3 mg/kg DiR-labeled NP or IF7-NP. After 0.5, 3, 6, 24, 48, or 72 h, the mice were anesthetized and observed with an excitation bandpass filter at 710 nm and an emission filter at 780 nm. The exposure time for each image was 3 s. After imaging, the mice were killed and their tumors and other major organs and tissues (heart, liver, spleen, lung, kidney) were harvested and placed in 24-well plates for ex vivo imaging. The blocking effect of a 50-fold molar excess of IF7 on tumor tissue targeting was also evaluated.

In Vivo Tumor Vessel Targeting, Paclitaxel-Induced Apoptosis of Tumor ECs, and Tumor Tissue Necrosis. Mice bearing MCF-7/ADR tumors (250 mm^3) were injected via the caudal vein with coumarin 6-labeled IF7-PTX-NP or PTX-NP at PTX doses of 2.5 mg/kg. After 48 h, the tumors were removed and processed for cryostat sectioning (10 μm). The tumor vessels were stained with anti-VE-cadherin antibody and PE-Cy5-labeled goat anti-rabbit IgG antibody. The apoptosis of the tumor vascular ECs was detected with an ApopTag Red In Situ Apoptosis Detection Kit (Merck Millipore). The slides were observed under a CLSM for CD31 (PE-Cy5: excitation, 543 nm; emission, LP 650 nm), apoptosis (rhodamine: excitation, 543 nm; emission, bandpass 565−615 nm), and coumarin 6 (excitation, 488 nm; emission, bandpass 505−550 nm). Paraffin sections (4 μm) of the tumors were processed for hematoxylin and eosin (H&E) staining and histological examination. The blocking effect of a 50-fold molar excess of IF7 on tumor vessel targeting was also evaluated.

Anticancer Therapy in Mice with Resistant MCF-7/ADR Xenografts. The right flanks of BALB/c mice were inoculated with MCF-7/ADR cells (2×10^6). When the tumors reached ~100 mm^3 in volume, four doses of the appropriate drug were given, on days 1 (start of treatment), 5, 9, and 13, to the mice through the caudal vein. Nine groups (five mice for each treatment) were established in this study: (1) control (saline); (2) Taxol (1 mg/kg); (3) PTX-NP (1 mg/kg); (4) IF7-PTX-NP (1 mg/kg); (5) Taxol (1 mg/kg) + XR9576; (6) Taxol (8 mg/kg); (7) Taxol (8 mg/kg) + XR9576; (8) IF7-PTX-NP (1 mg/kg) + IF7; and (9) IF7-PTX-NP (1 mg/kg) + XR9576. In the combined treatment with free IF7, the peptide was coadministered with IF7-PTX-NP (1 mg/kg). In the combination treatments with the P-gp inhibitor, XR9576 (10 mg/kg) was administered orally to the mice, according to the literature,[33] 2 h before the paclitaxel formulation was given. The tumor volumes and mouse body weights were monitored throughout the study.

The tumor volumes (mm^3) were calculated as length × $width^2/2$. At the end of the study, the mice were killed and the tumors were removed and processed to generate paraffin sections. The tumor vessels were stained with anti-CD31 antibody. Tumor cell apoptosis was detected with the ApopTag Peroxidase In Situ Apoptosis Detection Kit (Merck Millipore). All microphotographs were taken with a Leica DFC 320 photomicroscope. The MVD and percentage of TUNEL-positive cells were analyzed with the *Image-Pro Plus 6.0* software (Media Cybernetics, Bethesda, MD).

Statistical Analysis. All statistical analyses were conducted with the *GraphPad Prism 5.0* software (La Jolla, CA). Differences between groups were examined with Student's *t* test or ANOVA with the Bonferroni's multiple-comparison test. Differences were considered significant if the *P* value was less than 0.05.

DOI: 10.1021/acs.bioconjchem.5b00283
Bioconjugate Chem. 2015, 26, 1702−1712

AUTHOR INFORMATION

Corresponding Authors

*E-mail: fangchao100@hotmail.com. Tel./fax: +86 21 64674721.

*E-mail: hongzhuan_chen@hotmail.com. Tel./fax: +86 21 64674721.

Author Contributions

#De-Hong Yu and Ya-Rong Liu contributed equally to this work.

Notes

The authors declare no competing financial interest.

ACKNOWLEDGMENTS

We are grateful for the financial supports from Major Program of the National Natural Science Foundation of China (No. 81330023), National Natural Science Foundation of China (Nos. 81170924 and 81302709), Shanghai Committee of Science and Technology (14DZ2260300), Shanghai Municipal Health Bureau Program (No. 2012Y343), and Xinhua Hospital Foundation (No. 13YJ19).

ABBREVIATIONS

DDS, drug delivery system; NP, nanoparticles; PTX, paclitaxel; HUVEC, human umbilical vein endothelial cells; MDR, multidrug resistance; ECs, endothelial cells; TEM, transmission electron microscopy; VEGF, vascular endothelial growth factor; AUC, area under the concentration−time curve; PEG, poly(ethylene glycol); MVD, microvessel density; HPLC, high performance liquid chromatograph; DLS, dynamic light scattering; FITC, fluorescein isothiocyanate; H&E, hematoxylin and eosin; CLSM, confocal laser scanning microscopy

REFERENCES

(1) Abdollahi, A., and Folkman, J. (2010) Evading tumor evasion: current concepts and perspectives of anti-angiogenic cancer therapy. *Drug Resist. Updates 13*, 16−28.

(2) Sato, H., Siddig, S., Uzu, M., Suzuki, S., Nomura, Y., Kashiba, T., Gushimiyagi, K., Sekine, Y., Uehara, T., Arano, Y., et al. (2015) Elacridar enhances the cytotoxic effects of sunitinib and prevents multidrug resistance in renal carcinoma cells. *Eur. J. Pharmacol. 746*, 258−266.

(3) Kerbel, R. S. (2008) Tumor angiogenesis. *N. Engl. J. Med. 358*, 2039−2049.

(4) Mullard, A. (2013) 2012 FDA drug approvals. *Nat. Rev. Drug Discovery 12*, 87−90.

(5) Weis, S. M., and Cheresh, D. A. (2011) Tumor angiogenesis: molecular pathways and therapeutic targets. *Nat. Med. 17*, 1359−1370.

(6) Jain, R. K., and Carmeliet, P. (2012) SnapShot: tumor angiogenesis. *Cell 149*, 1408−1408.

(7) Pasquier, E., Kavallaris, M., and André, N. (2010) Metronomic chemotherapy: new rationalefor new directions. *Nat. Rev. Clin. Oncol. 7*, 455−465.

(8) Clarke, J. M., and Hurwitz, H. I. (2013) Ziv-aflibercept: binding to more than VEGF-Aedoesmore matter? *Nat. Rev. Clin. Oncol. 10*, 10−11.

(9) Cook, K. M., and Figg, W. D. (2010) Angiogenesis inhibitors: current strategies and future prospects. *Ca-Cancer J. Clin. 60*, 222−243.

(10) Luo, L., Zhang, X., Hirano, Y., Tyagi, P., Barabás, P., Uehara, H., Miya, T. R., Singh, N., Archer, B., Qazi, Y., et al. (2013) Targeted intraceptor nanoparticle therapy reduces angiogenesis and fibrosis in primate and murine macular degeneration. *ACS Nano 7*, 3264−3275.

(11) Goel, S., Chen, F., Hong, H., Valdovinos, H. F., Hernandez, R., Shi, S., Barnhart, T. E., and Cai, W. (2014) VEGF121-conjugated mesoporous silica nanoparticle: a tumor targeted drug delivery system. *ACS Appl. Mater. Interfaces 6*, 21677−21685.

(12) Guo, Z., He, B., Jin, H., Zhang, H., Dai, W., Zhang, L., Zhang, H., Wang, X., Wang, J., Zhang, X., and Zhang, Q. (2014) Targeting efficiency of RGD-modified nanocarriers with different ligand intervals in response to integrin $\alpha v\beta 3$ clustering. *Biomaterials 35*, 6106−6117.

(13) Kang, T., Gao, X., Hu, Q., Jiang, D., Feng, X., Zhang, X., Song, Q., Yao, L., Huang, M., Jiang, X., et al. (2014) iNGR-modified PEG-PLGA nanoparticles that recognize tumor vasculature and penetrate gliomas. *Biomaterials 35*, 4319−4332.

(14) Yu, D. H., Ban, F. Q., Zhao, M., Lu, Q., Lovell, J. F., Bai, F., Wang, C., Guan, Y. Y., Luan, X., Liu, Y. R., et al. (2013) The use of nanoparticulate delivery systems in metronomic chemotherapy. *Biomaterials 34*, 3925−3937.

(15) Hatakeyama, S., Sugihara, K., Shibata, T. K., Nakayama, J., Akama, T. O., Tamura, N., Wong, S. M., Bobkov, A. A., Takano, Y., Ohyama, C., et al. (2011) Targeted drug delivery to tumor vasculature by a carbohydrate mimetic peptide. *Proc. Natl. Acad. Sci. U. S. A. 108*, 19587−19592.

(16) Chen, X., Fan, Z., Chen, Y., Fang, X., and Sha, X. (2013) Retro-inverso carbohydrate mimetic peptides with annexin1-binding selectivity, are stable in vivo, and target tumor vasculature. *PLoS One 8*, e80390.

(17) Hatakeyama, S., Shibata, T. K., Tobisawa, Y., Ohyama, C., Sugihara, K., and Fukuda, M. N. (2013) Tumor targeting by a carbohydrate ligand-mimicking peptide. *Methods Mol. Biol. 1022*, 369−386.

(18) Bocci, G., Di, Paolo. A., and Danesi, R. (2013) The pharmacological bases of the antiangiogenic activity of paclitaxel. *Angiogenesis 16*, 481−492.

(19) Pasquier, E., Honore, S., Pourroy, B., Jordan, M. A., Lehmann, M., Briand, C., and Braguer, D. (2005) Antiangiogenic concentrations of paclitaxel induce an increase in microtubule dynamics in endothelial cells but not in cancer cells. *Cancer Res. 65*, 2433−2440.

(20) Sun, W., Lv, C., Zhu, T., Yang, X., Wei, S., Sun, J., Hong, K., Zhu, W., and Huang, C. (2013) Ophiobolin-O reverses adriamycin resistance via cell cycle arrest and apoptosis sensitization in adriamycin-resistant human breast carcinoma (MCF-7/ADR) cells. *Mar. Drugs 11*, 4570−4584.

(21) Veronese, F. M., and Pasut, G. (2005) PEGylation, successful approach to drug delivery. *Drug Discovery Today 10*, 1451−1458.

(22) Yu, D. H., Lu, Q., Xie, J., Fang, C., and Chen, H. Z. (2010) Peptide-conjugated biodegradable nanoparticles as a carrier to target paclitaxel to tumor neovasculature. *Biomaterials 31*, 2278−2292.

(23) Hofherr, S. E., Shashkova, E. V., Weaver, E. A., Khare, R., and Barry, M. A. (2008) Modification ofadenoviral vectors with poly-ethylene glycol modulates in vivo tissue tropismand gene expression. *Mol. Ther. 16*, 1276−1282.

(24) De, U., Chun, P., Choi, W. S., Lee, B. M., Kim, N. D., Moon, H. R., Jung, J. H., and Kim, H. S. (2014) A novel anthracene derivative, MHY412, induces apoptosis in doxorubicin-resistant MCF-7/Adr human breast cancer cells through cell cycle arrest and downregulation of P-glycoprotein expression. *Int. J. Oncol. 44*, 167−176.

(25) Wang, F., Wang, Y. C., Dou, S., Xiong, M. H., Sun, T. M., and Wang, J. (2011) Doxorubicin-tethered responsive gold nanoparticles facilitate intracellular drug delivery for overcoming multidrug resistance in cancer cells. *ACS Nano 5*, 3679−3692.

(26) Lu, L., Zhou, D., Jiang, X., Song, K., Li, K., and Ding, W. (2012) Loss of E-cadherin in multidrug resistant breast cancer cell line MCF-7/Adr: possible implication in the enhanced invasive ability. *Eur. Rev. Med. Pharmacol. Sci. 16*, 1271−1279.

(27) Wang, J., Qu, H., Jin, L., Zeng, W., Qin, L., Zhang, F., Wei, X., Lu, W., Zhang, C., and Liang, W. (2011) Pegylated phosphotidyle-thanolamine inhibiting P-glycoprotein expression and enhancing retention of doxorubicin in MCF7/ADR cells. *J. Pharm. Sci. 100*, 2267−2277.

(28) Li, Q. Q., Cao, X. X., Xu, J. D., Chen, Q., Wang, W. J., Tang, F., Chen, Z. Q., Liu, X. P., and Xu, Z. D. (2009) The role of P-glycoprotein/cellular prion protein interaction in multidrug-resistant breast cancer cells treated with paclitaxel. *Cell. Mol. Life Sci. 66*, 504−515.

DOI: 10.1021/acs.bioconjchem.5b00283
Bioconjugate Chem. 2015, 26, 1702−1712

(29) Bai, F., Wang, C., Lu, Q., Zhao, M., Ban, F. Q., Yu, D. H., Guan, Y. Y., Luan, X., Liu, Y. R., Chen, H. Z., et al. (2013) Nanoparticle-mediated drug delivery to tumor neovasculature to combat P-gp expressing multidrug resistant cancer. *Biomaterials 34*, 6163−6174.
(30) Kelly, R. J., Draper, D., Chen, C. C., Robey, R. W., Figg, W. D., Piekarz, R. L., Chen, X., Gardner, E. R., Balis, F. M., Venkatesan, A. M., et al. (2011) A pharmacodynamic study of docetaxel in combination with the P-glycoprotein antagonist tariquidar (XR9576) in patients with lung, ovarian, and cervical cancer. *Clin. Cancer Res. 17*, 569−580.
(31) Bauer, M., Zeitlinger, M., Todorut, D., Böhmdorfer, M., Müller, M., Langer, O., and Jäger, W. (2013) Pharmacokinetics of single ascending doses of the P-glycoprotein inhibitor tariquidar in healthy subjects. *Pharmacology 91*, 12−19.
(32) Pastorino, F., Brignole, C., Marimpietri, D., Cilli, M., Gambini, C., Ribatti, D., Longhi, R., Allen, T. M., Corti, A., and Ponzoni, M. (2003) Vascular damage and anti-angiogenic effects of tumor vessel-targeted liposomal chemotherapy. *Cancer Res. 63*, 7400−7409.
(33) Mistry, P., Stewart, A. J., Dangerfield, W., Okiji, S., Liddle, C., Bootle, D., Plumb, J. A., Templeton, D., and Charlton, P. (2001) In vitro and in vivo reversal of P-glycoprotein-mediated multidrug resistance by a novel potent modulator, XR9576. *Cancer Res. 61*, 749−758.

DOI: 10.1021/acs.bioconjchem.5b00283
Bioconjugate Chem. 2015, 26, 1702−1712